SCIENCE BULLETIN
CHIAO-TUNG UNIV.
Vol. 3, No. 2, 1969)

# Interface Study of Metal-Semiconductor Systems

by

C.Y.Chang *and S.M. Sze**

Abstract-Interface effect and carrier transport in metal-semiconductor systems have been studied theoretically and experimentally to give a generalized and quantitative presentation. The thermionic and tunneling processes have been analyzed in terms of the most accurate quantum transmission coefficients. The effects of image-force lowering, interface states, temperature, and two-dimensional statistical variation of impurity concentration have also been incorporated in the study.

The ohmic or rectifying behavior of a given metal-semiconductor system depends strongly on the temperature and doping concentration. The saturation current density $J_s$ is found to reach a minimum at a particular doping, e.g. for PtSi-Si system at 300°K with a barrier height of 0.85eV, $J_s$ is 80 na/cm$^2$ at $10^{14}$ cm$^{-3}$, reaches a minimum of 60 na/cm$^2$ at $10^{16}$ cm$^{-3}$, then rapidly increases to $10^3$ amp/cm$^2$ at $10^{20}$ cm$^{-3}$. At high doping range the average saturation current density will be considerably increased due to the effect of two-dimensional impurity variation.

The room-temperature transition doping for breakdown in metal-silicon system occurs at $8 \times 10^{17}$ cm$^{-3}$; for lower dopings the breakdown is due to avalanche multiplication, and for higher dopings due to tunneling of carriers from metal Fermi level to semiconductor band edges.

The metal-silicon diodes are fabricated by planar technology with guard-ring structures to eliminate edge effects. Extensive experimetal studies including current-voltage, and photoelectric messurements covering doping range from $10^{14}$ to $10^{20}$ cm$^{-3}$ and

* Now with College of Engineering, National Chiao-Tung University, Hsinchu, Taiwan, Republic of China

** Now with Bell Labs, Murray Hill, New Jersey, U.S.A.

temperature range from 77°K to 373°K give good agreement with theoretical predictions. Differentiation measurement at 4.2°K also reveals scatterings of phonons with interface states and phonon-phonon interaction between different valleys along the <100> axis.

## I. Introduction

Metal-semiconductor diode is one of the most important solid-state devices. It behaves similarly to a one-sided abrupt p-n junction, and yet it can be operated as a majority-carrier device with inherent fast response and radiation resistances. It has been extensively used in communication systems and digital computers. It has also shown its potential as useful microwave generator e.g. metal-semiconductor IMPATT diode [1], optoelectronic devices (e.g. Schottky barrier avalanche photodiode [2], and field-effect devices (e.g. Schottky-barrier-gate FET [3], and Schottky-contact IGFET [4].

The investigation of metal-semiconductor systems can be dated back to 1874 when Braun [5] first noted the dependence of the total resistance on the applied voltage. In 1938 Schottky [6] suggested the formation of surface barriers between metal and semiconductor contacts. In 1942 the basic thermionic emission theory was proposed by Bethe [7]. The analysis of rectifying contacts and experimental work prior to 1957 were summarized by Henisch [8]. Recent theoretical and experimental developments have been reviewed by Sze [9].

In the analysis of carrier transport in a metal-semiconductor system, both the diffusion theory by Schottky [6] and the thermionic emission theory by Bethe [7] have neglected the contribution of the tunneling current. Recently Padovani and Stratton [10] considered the tunneling component in terms of a field-emission model and obtained results for low-temperature condition. Crowell and Rideout [11] also considered the transport processes based upon the Boltzmann distribution and WKB approximation for the quantum transmission coefficient. In the above approaches [11] a combined parameter $(T/\sqrt{N})$ is used where T is the temperature and N is the doping concentration of the semiconductor; and their results are applicable for the case of low doping and moderately high temperatures. Crowell and Sze [12] proposed a thermionic emission-diffusion theory which gave a synthesis of Schottky's diffusion theory and Bethe's thermionic emission theory; and the result is applicable for low and moderete doping cases.

The present study gives a generalized approach which covers for the first time the complete spectrum of temperature from low

to high ranges and impurity concentration from weakly doped to degenerate cases. The present study differs from the previous approaches in the following aspects: (1) an accurate quantum transmission function based upon numerical computation is used for the complete energy range, (2) the Fermi-Dirac distribution function is used to take into account the degenerate cases, (3) the temperature and the doping concentration are considered as two independent parameters since the combined parameter $T/\sqrt{N}$ is useful only for limited ranges, and (4) a two-dimensional statistical variation of impurities is incorperated in the transport study.

The detailed transport analysis is presented in Sec. II which also includes studies of tunneling breakdown, ohmic behavior under degenerate condition, electron-phonon scattering, and interface states effect. The experimental results including differentiation measurement of interface states are presented in Sec. III. Discussion and conclusion are given in Sec. IV.

## II. Basic Transport Analysis

We shall consider in this section (1) the quantum transmission coefficient, (2) the carrier transport equation, (3) the two-dimensional impurity variation, and (4) the breakdown voltage as a function of doping and temperature.

The basic energy-band digram of a metal-n-type semiconductor system is shown in Fig. 1. The basic set of equations for the system can be given as follows [9]:

$$\phi_{Bn} = V_{bo} + V_n - \triangle\phi \tag{1}$$

$$E_m = \sqrt{2qN(V_{bo} - V - kT/\varepsilon_s}} \tag{2}$$

$$W = \sqrt{\frac{2\varepsilon_s}{qN}\left(V_{bo} - V - \frac{kT}{q}\right)} \tag{3}$$

$$\triangle\phi = \sqrt{\frac{qE_m}{4\pi\varepsilon_s}} \tag{4}$$

and

$$1/c^2 = 2\left(V_{bo} - V - \frac{kT}{q}\right)/(q\varepsilon_s N) \tag{5}$$

where $\phi_{Bn}$ is the barrier height, $V_{bo}$ the built-in potential at zero bias, $V_n$ the potential difference between the Fermi energy and the bottom of conduction band, $E_m$ the maximum electric field, N the doping concentration, V the applied voltage, W the depletion width, and C the differential capacitance per unit area.

1. Quantum Transmission Coefficient

The exact transmission coefficient can be obtained by solving the Schrodinger equation for the potential profile of a metal-semiconductor system:

$$-\frac{k^2h^2}{2m^*}\nabla^2\psi+\left[\frac{-q^2N}{2\varepsilon_s}\left(Wx-\frac{x^2}{2}\right)-\frac{q^2}{16\pi\varepsilon_s x}\right]\psi=E\psi \tag{6}$$

where the first two terms in the square bracket give the diffusion potential energy while the last term is the image force potential energy. We shall use the potential energy maximum $q\phi_{Bn}$ as a reference; and designate $\eta$ as energy measured downward from the reference, and $\zeta$ as energy measured upward (see Fig. 1.) The transmission coefficients have been computed based on the Tayler expansion method [13]. The results of the transmission coefficients are shown in Fig. 2. For electron energy less than that of the barrier maximum, the transmission function $T(\eta)$ is a monotonically increasing function of electric field, while for electron energy in excess of the barrier maximum the transmission function, $T(\zeta)$is a monotanically decreasing function of field, For electron energy exactly corresponds to the barrier maximum, or $\eta=\zeta=0$, the transmission coefficient is not unity,but varies from 6% at $10^3$ V/cm to 17% at $10^6$ V/cm.

The exact transmission coefficient will be used in the transport analysis. The transmission coefficient shown in Fig.2 covers the energy range near the potential maximum where the WKB approximation can not be used. For energies far below the potential maximum where the potential varies slowly with distance, however the WKB approximation can adequately give the transmission coefficient. The WKB transmission coefficient incorporating the image force correction is given by

$$T(\eta)=\exp\left\{-R\left[V_b^{\frac{1}{2}}(\eta+\triangle\phi)^{\frac{1}{2}}-(V_b-q\triangle\phi)\ln\frac{(V_b-q\triangle\phi)^{\frac{1}{2}}}{(V_b-q\triangle\phi+\eta)^{\frac{1}{2}}}\right]\right\} \tag{7}$$

where

$$R=\sqrt{\frac{4m^{*}\varepsilon_{s}}{\hbar^{2}N}} \tag{7a}$$

is a material parameter, and $V_b$ the diffusion barrier potential at bias V. $V_b$ and $\eta$ are measured in units of eV.

For electron energies in excess of the potential maximum the transmission coefficient (as shown in Fig. 2) is fitted by numerical method using a polynomial of order of ten.

Equation (7) is plotted in Fig. 3 for some typical field-doping combinations. The result is also extrapolated to $\eta = 0$ in order to make a comparison with the exact transmission function: We note that for dopings higher than $10^{16}$ cm $^{-3}$ (i.e. for $R \leq 1000eV^{-1}$ ) the agreement is good, so that a match between the exact transmission function and the WKB result can be made at relatively large transmission coefficient near the potential maximum. At lower dopings (i.e. $R > 1000eV^{-1}$) the agreement is poor hence the exact transmission function should be used until the transmission coefficient becomes vanishingly small.

## 2. Carrier Transport Equation

In order to compare the present theory with the previous approaches[10-12], we shall divide the transport processes into thermionic and tunneling components.

The current density equation of carriers traversing from the semiconductor to the metal is proportional to the transmission coefficient multiplied by the occupation probability in the semiconductor and the unoccupied probability in the metal, i.e.

$$J_{SM}=\frac{A^{*}T}{k}\int_{0}^{V_b-\triangle\phi} F_s(V)T(\eta)(1-F_m)d\eta + \frac{A^{*}T}{k}\int_{0}^{\infty} T(\zeta)\exp-\frac{(V_b+V_n+\zeta+\triangle\phi)}{kT}\,d\zeta \tag{8}$$

where the first term corresponds to the tunneling component and the second term the thermionic component. $F_S$ and $F_m$ are the Fermi-Dirac distribution functions for the semiconductor and the metal respetively

$$F_m = \frac{1}{1 + \exp\left(\frac{V_{bo} - \eta + V_n}{kT}\right)} \tag{9}$$

$$F_s = \frac{1}{1 + \exp\left(\frac{V_{bo} - \eta + V_n - V}{kT}\right)} \tag{10}$$

and A* is the effective Richardson constant, T the temperature, K the Boltzmann constant, and $T(\eta)$ and $T(\zeta)$ the transmission coefficients below and above the potential maximum respectively.

The calculated results of $J_{SM}$ versus V are shown in Fig. 4. The experimental data are also presented but will be discussed in Sec. III.

The constants used in the calculation are: $A^* = 240$ amp/cm$^2$ / $^oK$, $m^* = 0.3\ m_o$, $\varepsilon_s = 11.8\ \varepsilon_o$ and $q\phi_{Bn} = 0.8$eV. (for Au-nSi). At 300$^o$K, the curve for $10^{16}$cm$^{-3}$ is the lowest.
The current density at $10^{18}$cm$^{-3}$ is about 20 times larger than that for $10^{16}$ cm$^{-3}$. At 77$^o$K, the curve for $10^{16}$ cm$^{-3}$ is also the lowest one. The current density at $10^{18}$ cm$^{-3}$ is now more than 5000 times greate than that at $10^{16}$ cm$^{-3}$.

The current density equation of carriers traversing from the metal to the semiconductor is

$$J_{MS} = \frac{A^*T}{k} \int_o^{V_b - \triangle\phi} F_m T(\eta)(1 - F_s)\, d\eta + \frac{A^*T}{k} e^{-\frac{q\phi_B}{kT}} \int_o^{\infty} T(\zeta) e^{-\zeta/kT}\, d\zeta \tag{11}$$

The thermionic component in $J_{MS}$ i.e., the second term in Eq. (9), is almost constant independent of voltage since the barrier height $\phi_B$ is essentially independent of voltage. However, due to the image-force lowering, this term will slightly increase when the reverse biase is increased.

At very high dopings and low temperatures, the tunneling component will dominate, and the current $J_{MS}$ will increase more rapidly with respect to the voltage.

The I-V characteristics at 300$^o$K under reverse biased condition are shown in Fig. 5 for dopings of $10^{14}$cm$^{-3}$ to $10^{17}$ cm$^{-3}$. Experimental results are also presented which will be discussed

later.

The total current density is given by the difference of Eqs.(8) and (11):

$$J_{Q.E.} = J_{SM} - J_{MS} \tag{12}$$

and the saturation current density can be obtained by setting $V = 0$ in Eq. (8) or (11):

$$J_s = \frac{A^*T}{k} \int_0^{V_{bo} - \Delta\phi} F_m T(\eta)[1 - F_s(V=0)]d\eta + \frac{A^*T}{k} \int_0^{\infty} T(\zeta) e^{-(V_{bo} + V_n + \zeta - \Delta\phi)/kT} d\zeta \tag{13}$$

The values of $J_s$ versus N are shown in Fig. 6 for Au-n-type Si and PtSi-n-type Si systems (in which $q\phi_{Bo} = 0.85eV$).

The values of the saturation current density $J_s$ as a function of doping are shown in Fig. 6 for Au-Si and PtSi-Si systems. It is interesting to note the variation of $J_s$ with doping. For example for Au-Si system at 300°K, $J_s$ is $4 \times 10^{-7}$ amp/cm$^2$ for N= $10^{14}$cm$^{-3}$, reaches a minimum value of $3\,6 \times 10^{-7}$ amp/cm$^2$ at $10^{16}$cm$^{-3}$, then increases monotonically to $4 \times 10^{-3}$ amp/cm$^2$ at $10^{19}$cm$^{-3}$ and $1.2 \times 10^{3}$ at $10^{20}$ cm$^{-3}$.

The ratio of tunneling to thermionic current component is

$$S \equiv \frac{J_t}{J_{th}} = \frac{\int_0^{V_b - \Delta\phi} T(\eta)(F_s(V) - F_m)\,d\eta}{\int_0^{\infty} T(\zeta) e^{-(V_b + \zeta + V_n - \Delta\phi)/kT} d\zeta} \tag{14}$$

A plot of S versus N is shown in Fig. 7. The value of S varies over 18 orders of magnitude for samples with doping of $10^{14}$cm$^{-3}$ at 375°K to $10^{18}$cm$^{-3}$ at 77°K. Increasing of doping and decreasing of termperature will always increase the tunneling component.

From the slope of the current-voltage characteristics, one can easily define a parameter n such as

$$n \equiv \frac{q}{kT} \frac{1}{\left(\frac{d\ell nJ}{dV}\right)}$$

A plot of the parameter n is shown in Fig. 8. The value of n increases with doping concentration but decreases with temperature. For example for a doping of $10^{18}$ $cm^{-3}$, the value of n is 1.08 at $300^{o}K$ and increases to 1.57 at $77^{o}K$.

3. Two Dimensional Statistical Effect

Because of the statistical nature of impurity distribution in the sample, the measured saturation current density for a given average doping concentration will deviate from the ideal values obtainable from Eq. 13 .

One can define a deviation width in doping by $\triangle N_o$ where $\triangle$ is the deviation percentage, $N_o$ the average doping concentration obtained from resistivity measurement. If one assumes a Gaussian distribution for the variation of impurity concentration, one obtains the elementary area dA as

$$dA = \frac{A}{\sqrt{\pi}\triangle N_o} \exp\left[-\left(\frac{N-N_o}{\triangle N_o}\right)^2\right] dN \tag{15}$$

Where A is the total device area.

The expectation value of the saturation current density is given by

$$J_s = \frac{1}{A}\int_{-\infty}^{\infty} J_s(N)\, dA = \int_{-\infty}^{\infty} \frac{1}{\sqrt{\pi}\triangle N_o} J_s(N) \exp\left[-\left(\frac{N-N_o}{\triangle N_o}\right)^2\right] dN \tag{16}$$

where $J_s$ (N) is the variation of the saturation current with doping for the ideal case. The functional form of $J_s$ (N) can be obtained from Fig. 6 (solid and dashed lines), by numerical mothod. The computed fesult for $J_s$ versus N for Au-Si system at $300^{o}K$ is also shown in Fig. 6 (dotted lines). When $\triangle = 0.1$ the values of $\langle J_s \rangle$ are essentially the same as that for the ideal case. When $\triangle = 0.5$, however $\langle J_s \rangle$ becomes 10% larger than the ideal $J_s$ at $10^{18}$ $cm^{-3}$ and is over 100% larger then the ideal $J_s$ at $10^{19} cm^{-3}$

4. Breakdown Voltages

For Schottky barriers, the breakdown mechanism is due to avalanche multiplication for weakly doped samples and due to tunneling for heavily-doped samples. The avalanche breakdown is essentially the same as that for one-sided abrupt junctions and the breakdown voltage is given by

$$V_B = \frac{\varepsilon_s E^2_m}{2qN} - \phi_{Bn} - V_n \tag{17}$$

where $E_m$ is the maximum field strength at breakdown which is slightly dependent on doping and temperature.[14,15] For heavely-

doped samples, the tunneling component will dominate the transport process. We shall define the breakdown voltage at which the reverse current density becomes 5000 $J_{smin}$. Where $J_{smin}$ is the minimum saturation current density for the metal-semiconductor system, e.g. for Au-Su system at 300°K $J_{smin}$ is $3.6 \times 10^{-7}$ amp/cm$^2$.

The theoretical result of breakdown voltage for Schottky barriers is shown in Fig. 9. For the avalanche multiplication process, the breakdown voltage increases with increasing temperature, e.g. for $N = 10^{16}$cm$^{-3}$. $V_B$ is 56 volts at 250°K and increases to 60 volts at 350°K. On the other hand, for tunneling process, the breakdown voltage decreases with increasing temperature, e.g. for $N = 4 \times 10^{18}$cm$^{-3}$, $V_B$ is about 0.7V at 300°K and decreases to 0.1V at 350°K.

In the previous section we have implicitely assumed that the carrier mean free path is infinite so that collisions in the depletion layer can be neglected. In this section we shall derive transport equations which incorporate the effect of carrier scatterings within the depletion layer.

## Ⅲ. Quantum Emission-Diffusion Theory and Related Scattering Processes

### 1. Quantum Emission-Diffusion Theory

In quantum emission-diffusion (QED) theory the following assumptions are made: (1) there is no interaction between the quantum emission and the diffusion mechanism, (2) the total current is determined by the combined conductance of the two series conductances resulting from the above two machanisms, (3) the diffusion mechanism occurs only within the range from the emitted band edge to the barrier minimum.

Based on the assumptions (1) and (2), one obtains for the total current density:

$$J = \frac{J_{QE} J_D}{J_{QE} + J_D} \tag{18}$$

where $J_{QE}$ is the quantum-emission current, and $J_D$ is the diffusion current. The diffusion velocity can be obtained from assumption (3), and the result is similar to that given by Crowell and Sze: [12]

$$V_D = \left[ \int_{x_E}^{w} \bar{D}^{-1} \exp\left[ -qV(\chi)/kT \right] d\chi \right. \tag{19}$$

where $\bar{D}$ is the average diffusion coefficient, V ($\chi$) the barrier potential, and $\chi_E$ as shown in Fig. 1 is the position at which maximum amount of carrier transport occurs. The $\chi_E$ is given as: [10]

$$\chi_E = W\left[1 - \cosh^{-1}\left(\frac{1}{RKT}\right)\right] \tag{20}$$

According to Crowell and Sze, [12] the ratio of $J_{QE}$ and $J_D$ can be approximated by the ratio of the recombination velocity and the diffusion velocity, i.e. $J_{QE}/J_D = V_R/V_D$. Hence the total current density becomes

$$J = \frac{J_{QE}}{1 + V_R/V_D} \tag{21}$$

where the recombination velocity is

$$V_D = \frac{A^* T^2}{qN_C} \tag{22}$$

It is obvious that when $\chi_E$ equals zero, i.e. at the potential barrier maximum, equation (18) will automatically reduce to the result of Crowell and Sze's thermionic emission-diffusion theory. However, when tunneling dominates, $x_E$ will occur at the lower band edge. When RKT tends to zero (i.e. tunneling dominates) $\chi_E$ will tend to W and thus the diffusion mechanism becomes less important.

2. Electron-phonon Scattering

In an electron-phonon scattering event the conservation of wave vector should be held:

$$q = k' - k - g \tag{23}$$

where q is the phonon momentum, k the electron momentum before scattering, and k' the electron momentum after scattering. g is the reciporcal lattice vector. Inan electron-phonon scattering event there are two kinds of processes: (1) the N-process with $g = 0$ which makes the scattering matrix element vanishes [16] for transverse wave thus only the longitudinal phonon scattering is possible, and (2) the U-process with $g \neq 0$, hence both the transverse and the longitudinal phonons are involved.

It is believed that when the period of a lattice vibration is much larger than the electron relaxation time, $\tau$, then the scattering of electrons by phonons, giving rise to conductance (or resistance) peaks will occur. From this creterion [16] one obtains

$$T < K/kT. \tag{24}$$

At low temperatures this condition is fulfilled. At extremely low temperature, e.g. at liquid helium temperature (see Sec. IV - 4), excitation of phonons can be made by biasing or neutron diffraction [17, 18].

In order to observe the excited phonons, measurements of differential conductance as well as $\frac{d^2I}{dV^2}$ of the metal-semiconductor systems have been performed at liquid helium temperature.

3. Interface State Emission and Recombination

The capture and emission of majority carriers by the interface states will also contribute to the differential conductance when a d.c. bias is applied on the metal-semiconductor system similar to that as in the MOS structure. According to Nicollan and Geotzberger's results [19] for MOS structure, the interface-state conductance is given by

$$G = \frac{qN_t F_o \frac{\partial F_o}{\partial E} W^2 \tau^2}{1 + W^2 \tau^2} \tag{25}$$

where $N_t$ is the interface-state density, $F_o$ the distribution function in equilibrium, E the electron energy, $\tau$ the time constant, and $\omega$ the angular frequency of the applied small a.c. signal. The variation $\frac{\partial F_o}{\partial E}$ is a maximum when the Fermi level coincides with the energy of the interface state $E_t$. Thus the differential conductance peak gives the position of interface state in the semiconductor band gap.

## IV. Experimental Procedure and Results

1. Device Fabrication

The metal-semiconductor devices are fabricated on n-type, <111> oriented, one-side polished, low-dislocation-density silicon wafers. For samples with doping concentrations above $10^{16}$ cm$^{-3}$, single crystal wafers are used; for lower dopings epitaxial wafers of n on $n^+$ are used in order to reduce the series resistance. To eliminate the edge effect, a guard ring structure has been used. The device geometry is shown in Fig. 10. The fabrication procedure is essentially the same as that described by Lepselter and Sze [20]

using plannar technology.

The sample is cleaned first. After oxidation to grow a oxide of 5000 Å, a guard-ring window is opened in the oxide by the use of photoresist techique. Boron is then diffused into the window to form a $p^+$ guard ring with junction depth of 5 $\mu$m. (an ohmic contact is made on the back side of the sample by alloy method.) A window inside the guard ring is opened in the oxide, and gold film of about 1000 Å is evaporated onto the window to form the metal-semiconductor contact. The effective areas of the contacts are $4 \times 10^{-5}$, $3 \times 10^{-4}$, and $2 \times 10^{-3}$ $cm^2$. Another photoresist process is used to isolate the metal contacts from one another. For PtSi-Si devices, the platinum silicide is formed by deposition of Pt using back sputtering method and then sintering at 600°C inside the vacuum system. Most of the devices are bonded by thermal compression method on TO-5 packages so that they can be measured at various temperatures.

2. Current-Voltage and Capacitance-Voltage Measurements

The current-voltage measurement setup includes an HP 425 micro-volt-ammeter and a United System Corporation Model 211 digital voltmeter. A Boonton 74D capacitance bridge is used for the capacitance voltage measurement.

The measured forward-biased I-V curves are shown in Fig. 4(a) for 296°K and Fig. 4(b) for 77°K. We note that there is general agreement between the experimental results and the theoretical predictions. The deviations of current at lower voltages at 77°K is presumbly due to recombination-generation effect in the depletion region. The effect of two-dimensional statistical variation of impurities can be clearly seen from these figures, i.e. for samples of $10^{18}$ $cm^{-3}$ the experimental data are considerably higher than the theoretical curves for uniformly doped ideal samples. The variation of the saturation current density $J_s$ with doping is plotted in Fig. 6 for Au-Si devices measured at room temperature. There is also excellent agreement between theory and experiment.

The reverse-biased curves are shown in Fig. 5. The measured reverse currents are fairly close to the theoretical values except the sample of $10^{14}$ $cm^{-3}$ in which a large contribution of recombination-generation current component is expected. The values of the breakdown voltages, at which the reverse current increases rapidly with bias, are also in reasonable agreement with the predicted values as shown in Fig. 8.

The measured capacitances follow the expression given by Eq. (5). From the plots of $1/C^2$ versus V, the built-in potential $V_{bo}$

can be determined from the intercept on the voltage axis. The ionized impurity concentration can also be determined from the slope of the plot. Once the built-in potential $V_{bo}$ is determined and the voltage $V_n$ corresponding to the difference between the Fermi level and the conduction band edge is deduced from the doping concentration, the barrier hight is given as

$$\phi_{Bo} = V_{bo} + V_n - kT/q . \tag{26}$$

where $\phi_{Bo}$ is the intrinsic barrier height since in the capacitance method the built-in potential is not affected by the image force. The values of $\phi_{Bo}$ for Au-Si system at room temperature obtained from capacitance measurement are listed in Table I. The result shows that the intrinsic barrier height is about 0.8V and is independent of impurity concentration.

3. Photoelectric Measurement

It is well known that the photoelectric measurement is the most accurate method in determining the barrier height. When the square root of the photoresponse per absorbed photon is plotted against the photon energy, the intercept gives directly the value of the barrier height.

A Shimatzu spectrophotometer type GE 120 is used for the measurement. Some adjustment of the grating system is made in order to extend the wavelength to larger values. A 500W tungsten lamp is used as the light source. The measured result of $\phi_{Bn}$ is listed in Table II. Also listed are the barrier lowering due to image-force effect.[21] The intinsic barrier height which is the sum of $\phi_{Bn}$ and is given in the last column. It is obvious that the intrinsic barrier height $\phi_{Bn}$ over the doping range is essentially a constant; and the result is consistant with the capacitance measurement.

4. Differentiation Measurement

In order to study the scattering events in the transport processes, one of the most useful methods is the measurement of the first and the second derivatives of the current - voltage characteristics. The setup of the measurement is identical to that described by Patterson and Kuhn [22] in which a lock in detection system is used and the differential peaks are plotted on an X-Y recorder. The devices are mounted in TO-5 package which can be immersed directly into liquid helium.

The measured second derivatives are shown in Fig. 11(a) for PtSi-Si barrier and Fig. 11(b) for Au-Si barrier. It is interesting to observe that there are several peaks over the bias range of

about 100mV. The result is summarized in Table III. Of particlar interest are the peaks at 22 meV and 56 meV which are present for both systems and under forward and reverse biasing conditions.

## V. Discussion and Conclusion

The present study incorporating the accurate quantum transmission coefficients gives for the first time a generalized and quantitative result for the carrier transport in metal-semiconductor systems. Special emphasis has been placed on the importance of the impurity concentration whose effects are threefolds:

1. For a given metal-semiconductor system the saturation current density $J_s$ depends strongly on temperature and on the impurity concentration especially at dopings higher than $10^{17}$ $cm^{-3}$. Therefore even for a high-barrier system its rectifying or ohmic behavior can not be determined unless the impurity concentration is specified. For example the barrier height of PtSi-Si is about 0.85eV; it is a rectifying contact for lower dopings. However the value of $J_s$ at room temperature approaches $1.2 \times 10^3$ amp/$cm^2$ at $10^{20}$ $cm^{-3}$ due to tunneling effect. Such a large current density can well explain the ohmic-contact behavior between PtSi and a degenerate n-type silicon.
2. Becuase of the dependence of $J_s$ on doping, the evaluation of the barrier height from I-V measurement may result in considerable error. Therefore the photoelectric and capacitance measurements should be used for the determination of the barrier height.
3. Due to the two-dimensional statistical variation of impurity concentration, the measured current density for a given average doping is always larger in comparison to that computed for the ideal condition of uniformly doped sample. The difference becomes greater as the doping increases.

The experimental current-voltage characteristics as shown in Fig. 4, 5 and 6 are in quantitative agreement with the theoretical predictions. These results also show the importance in the use of the accurate quantum transmission coefficient and the Fermi-Dirac distribution function in the transport analysis.

We have considered the doping concentration N and the lattice temperature T as two independent parameters rather than a combined parameter (RKT) which is proportional to $T/\sqrt{N}$. A comparison of the present theory with that of Crowell and Rideout's theory [11] using the combined parameter is shown in Fig. 12. Where $J_f$ is the forward current density and $J_m \equiv A^*T^2 \exp(-qVn/$

KT) corresponding to the thermionic current density at flat band condition. We note that for RKT = 1.5 the two theories are in reasonable agreement. For RKT = 0.1, however, there are considerable difference between the two theories. In addition for a given RKT, one obtains different I-V characteristics for different combinations of T and N. It is thus clear that the combined parameter RKT is only applicable over limited range of T and N, and can not be used as a universal parameter especially for tunneling cases.

From the C-V measurement and photoelectric measurement it is confirmed that the intrinsic barrier height $\phi_{Bo}$ of Au-n-type Si system is a constant independent of doping concentration over the range $10^{14}$ to $10^{20}$ $cm^{-3}$.

In the differentiation measurement, a peak corresponding to the 56 meV transverse optical phonon is always observed in both forward and reverse biases for PtSi-Si and Au-Si diodes. However, the peak corresponding to the 18.4 meV transverse acoustic phonon is missing in the PtSi-Si diodes and in the Au-Si diode under forward bias, It is conceivable that the conservation of momentum in a metal-semiconductor system is not strictly valid, since phonons may interact with energy states which exist at the metal-semiconductor interface.

It is believed that because of the sintering process the crystalline structures of PtSi-Si interface are more orderly oriented, therefore there are less energy states present at the interface. For Au-Si diodes, however, because of the deposition process, one expects to have more interface states. The differential conductance peaks are listed in Table III. As expected, the Au-Si diode under forward bias shows the largest number of conductance peaks.

It is interesting to note that peak at 22 meV is present in both kinds of diodes and in forward and reverse bias conditions. But this peak does not exist in the conventional phonon spectra of p-n junction devices. According to Dumke's theory [23] deduced from Haynes optical data, the longitudinal acoustic phonon energy corresponding to scattering between valleys along the <100> axis is 23 meV. Therefore it is apparent that this kind of Scattering can be observed in metal-semiconductor systems.

Acknowledgements

We wish to express our deep gratitude to Prof. L. J. Chu for his constant encouragement during the course of the study. Thanks are also due to Prof. L. Y. Wei for his helpful suggestions, Prof. Y. T. Yang for the provision of the liquid helium setup at the National Tsing Hwa University, and to Prof. J. Y. Lee for his

assistance in computation work. The financial supports of the C. Y. Tung's Grant, the International Foundation, and the Nationál Science Council are greatly appreciated. We wish also to acknowledge technical assistance of Miss H. R. Hsu, Miss G. Y. Yang, Mr. M. S. Tang, and Mr. T. P. Wu in sample preparation and device measurement.

References

1. S. M. Sze, M. P. Lepselter, and R. W. MacDonald, "Metal-Semiconductor IMPATT Oiode,"Solid State Electron.,Vol.12,p.109 (1969).
2. H. Melchoir, M. P. Lepselter, and S. M. Sze, "Metal-Semiconductor Avalanche photodiode ", paper presented at IEEE Solid State Device Research Conf. Boulder, Colarado, June (1968).
3. C. A. Moad, "Schottky Barrier-gate Field Effect Transistor" Proc. IEEE, 54, 307 (1966).
4. M. P. Lepselter and S. M. Sze, "SB-IGFET: Field-Effect Transistor Using Schottky Barrier Contacts as Source and Drain." Proc. IEEE, Vol 56, p 1400 (1968).
5. F. Braun, "Ukey die Stremleitung durch Schwefelmetalle,"Ann. Physik Chem,, 153, 556 (1874).
6. W. Schottky, Natarwiss, 26, 843 (1938).
7. H. A. Bethe, "Theory of the Boundary Layer of Crystal Rectifier," MIT Radiation Laboratory, Report 43-12 (1942).
8. H. K. Henish,"Rectifier Semiconductor Contacts," Oxford at the Clarendon Press, Oxford (1957).
9. For a recent review on metal-semiconductor systems see, for example, S. M. Sze, Physics of Semiconductor Devices, John Wiley and Sons, New York (1969).
10. F. A. Padovani and R. Stratton, "Field and Thermionic-Field Emission in schottlcy Barriers", Solid State Blectron., Vol, 9 p 695 (1066).
11. C. R. Crowell and V. L. Rideout,"Normalized I-V Characteristic in Metal-Semiconduetor contact and zero bias anomalies" Solid State Electron., Vol. 12, p. 89 (1969).
12. C. R. Crowell and S. M. Sze, "Current Trensport in Metal - Semiconductor Barriers," Solid State Electron., Vol. 9, p 1035 (1966).
13. C. R. Crowell and S. M. Sze, "Ouantum Mechanical Reflection at Metal-Semiconductor Barriers," J. Appl. Phys., Vol. 37, p. 2683 (1966).
14. C. R. Crowell and S. M. Sze, Appl. Phys. Letters, Vol. 9, p242

(1966).
15. S. M. Sze and G. Gibbons, "Avalanche Breakdown Voltages of Abrupt and Linerly Graded p-n junctions in Ge, Si, GaAsand GaP," Appl. Phys. Letters, Vol. 8, p. 111 (1966).
16. J. M. Ziman, "Electrons and Phonons" p. 173, Oxford Univ. Press. (1958).
17. A. G. Chynoweth, R. A. Logan, and D. E. Thomas,"phonon-Assisted Tunneting in Silicon and Germanium Esaki Junctions," Phys. Rev. Vol. 125, p 877 (1962).
18. B. N. Brockhouse and P. K. Iyengar, "Normel Modes of Germainum by Neution Spectrometry." Phys. Rev. 111, p. 1273 (1958).
19. E. H. Nicolian and A. Geortzberger, "Mos Conductance Technique for Measuring Surface State Parameters," Bell Syst. Tech. J., Vol. 46, p. 1055 (1967).
20. M. P. Lepselter and S. M. Sze, "Silicon Schottky Barrier Diode with Neal-Ideal I-V Characteristics," Bell Syst. Tech. J., Vol. 47, p. 195 (1968).
21. S. M. Sze, C. R. Crowell, and D. Kahng,"photoelectric Determination of the Image Force Dielectric Constant for Hot Elertrons in Schottky Barriers,"J. Appl. Phys., Vol. 35, p. 2534 (1964).
22. W. R. Patterson and M. Kuhn, Advanced Research Projects Agency, Washington D. C. ARPA-E99 (1968).
23. W. P. Dumke, "Two phonon Indirect Transitions and Lattice Scattering in Si", Phys. Rev., Vol. 118, p. 938 (1960).

Table I. Capacitance Measurement of Intrinsic Barrier Height of Au-Si (at 300°K)

| Doping ($cm^{-3}$) | $V_{bo}$ (Volts) | $V_n$ (volts) | $\phi_{Bo}$ (volts) |
|---|---|---|---|
| $8.6 \times 10^{14}$ | 0.54 | 0.269 | 0.809 |
| $1.4 \times 10^{16}$ | 0.61 | 0.197 | 0.807 |
| $1.0 \times 10^{17}$ | 0.66 | 0.146 | 0.806 |
| $3.6 \times 10^{18}$ | 0.70 | 0.11 | 0.81 |

Table II. Photoelectric Measurement of Intrinsic Barrier Height of Au-Si System (at 300°K)

| Doping ($cm^{-3}$) | Resistivity ($\Omega$-cm) | $\phi_{Bn}$ (volts) | $\triangle\phi$(volts) | $\phi_{Bo}$ (volts) |
|---|---|---|---|---|
| $1.0 \times 10^{15}$ | 4.3 | 0.780 | 0.017 | 0.797 |
| $3.6 \times 10^{17}$ | 0.025 | 0.740 | 0.053 | 0.793 |
| $1.1 \times 10^{18}$ | 0.01 | 0.738 | 0.073 | 0.811 |

Table III. Differential Conductance Peaks (at 4.2°K)

| System | Biasing Condition | Energy (meV) |
|---|---|---|
| Au-Si | Forward | 6, 13, -, 22, -, 42, 46, 56, -, 74 |
| | Reverse | 18, 22, -, 42, -, 56, |
| PtSi-Si | Forward | 22, -, 42, -, 56, 72.6, 93 |
| | Reverse | 22, 35, -, -, 56, 68 |

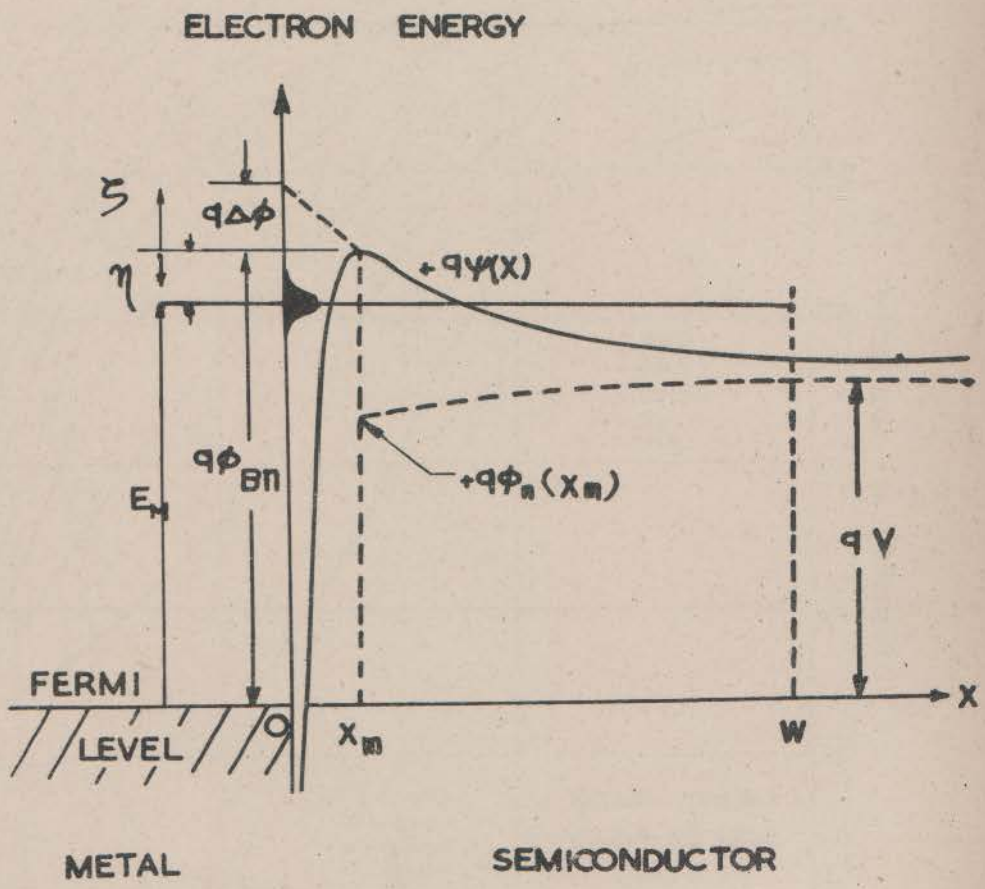


Fig. 1. Band diagram of a metal-semiconductor system.

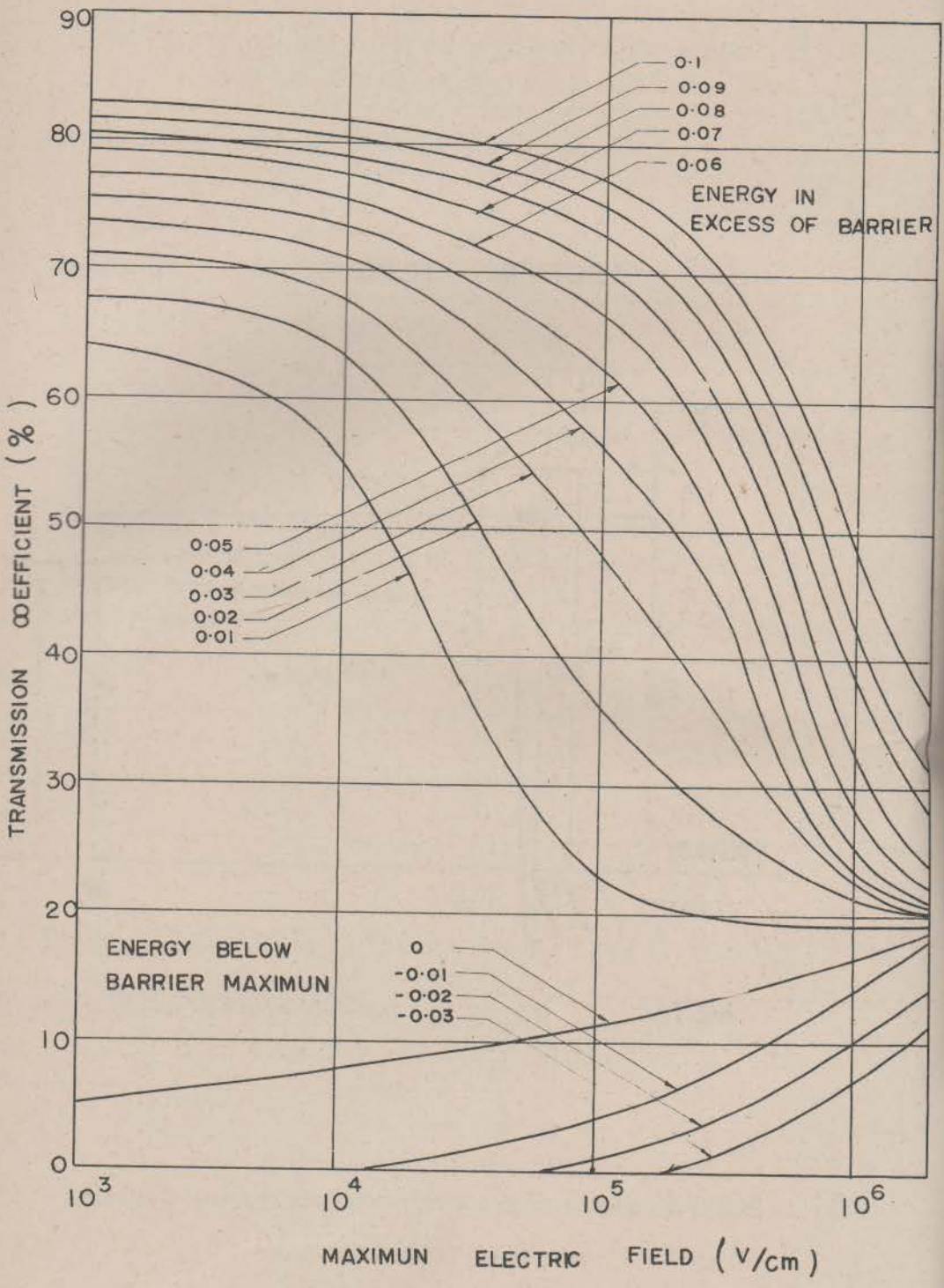


Fig. 2. Transmission coefficient versus electric field with electron energy as a parameter.

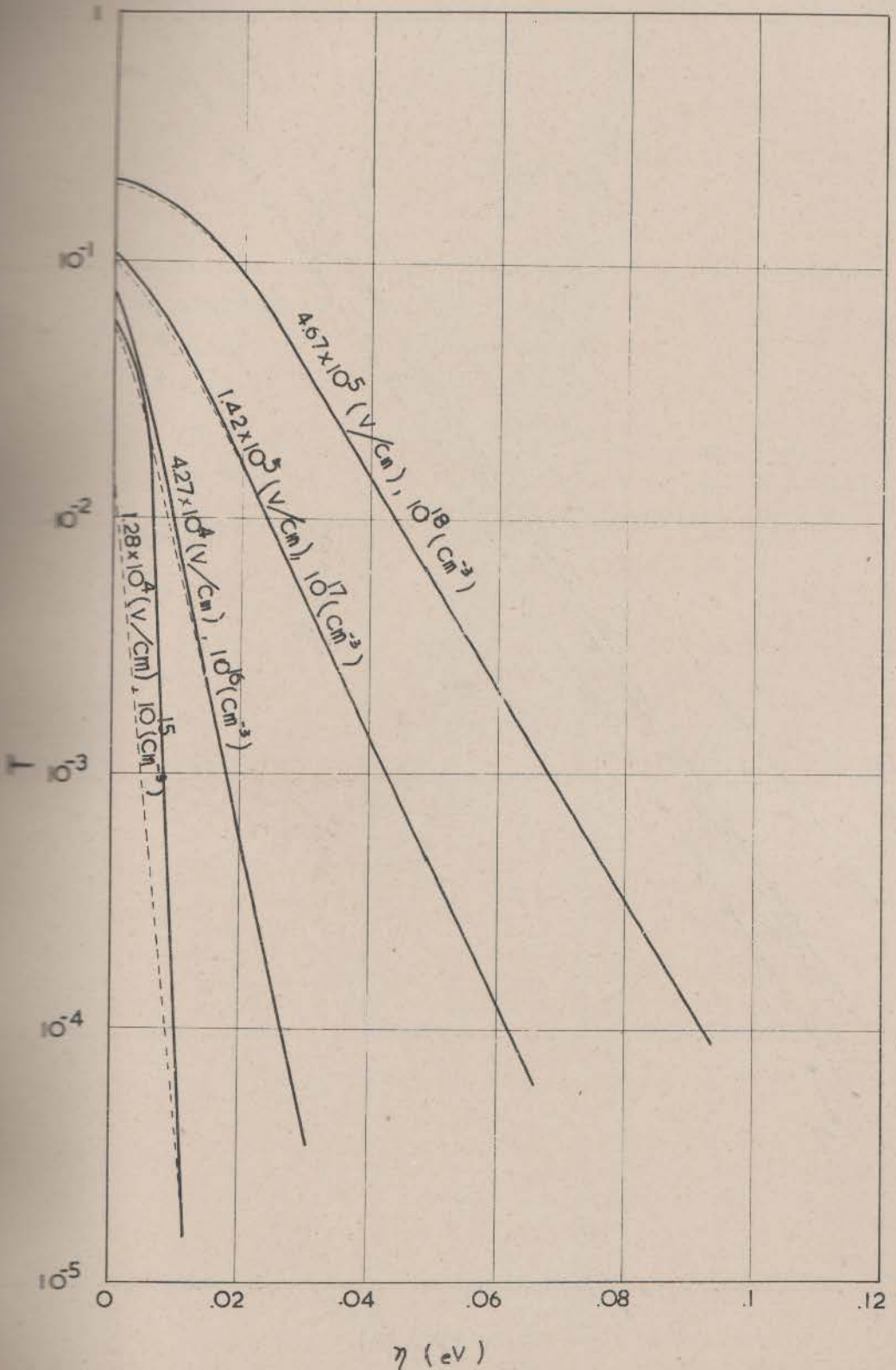


Fig. 3. Comparison of $T(\eta)$ with the exact quantum transmission coefficient for energies below the potential maximum.

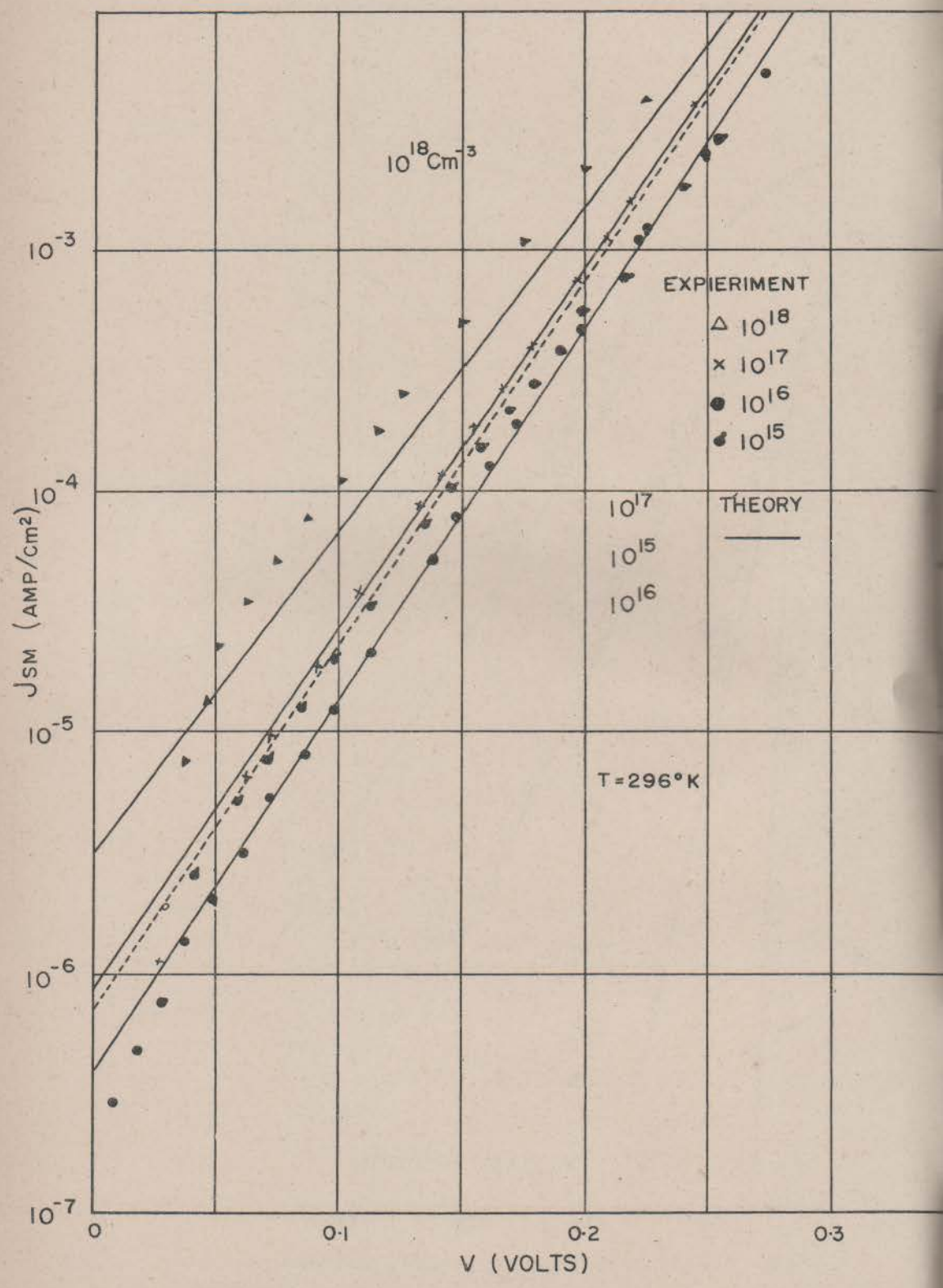


Fig. 4. Theoretical and experimental values of $J_{SM}$ versus forward applied voltage. Solid lines are the theoretical results and the data points are obtained experimentally.
(a) for T = 296°K, and

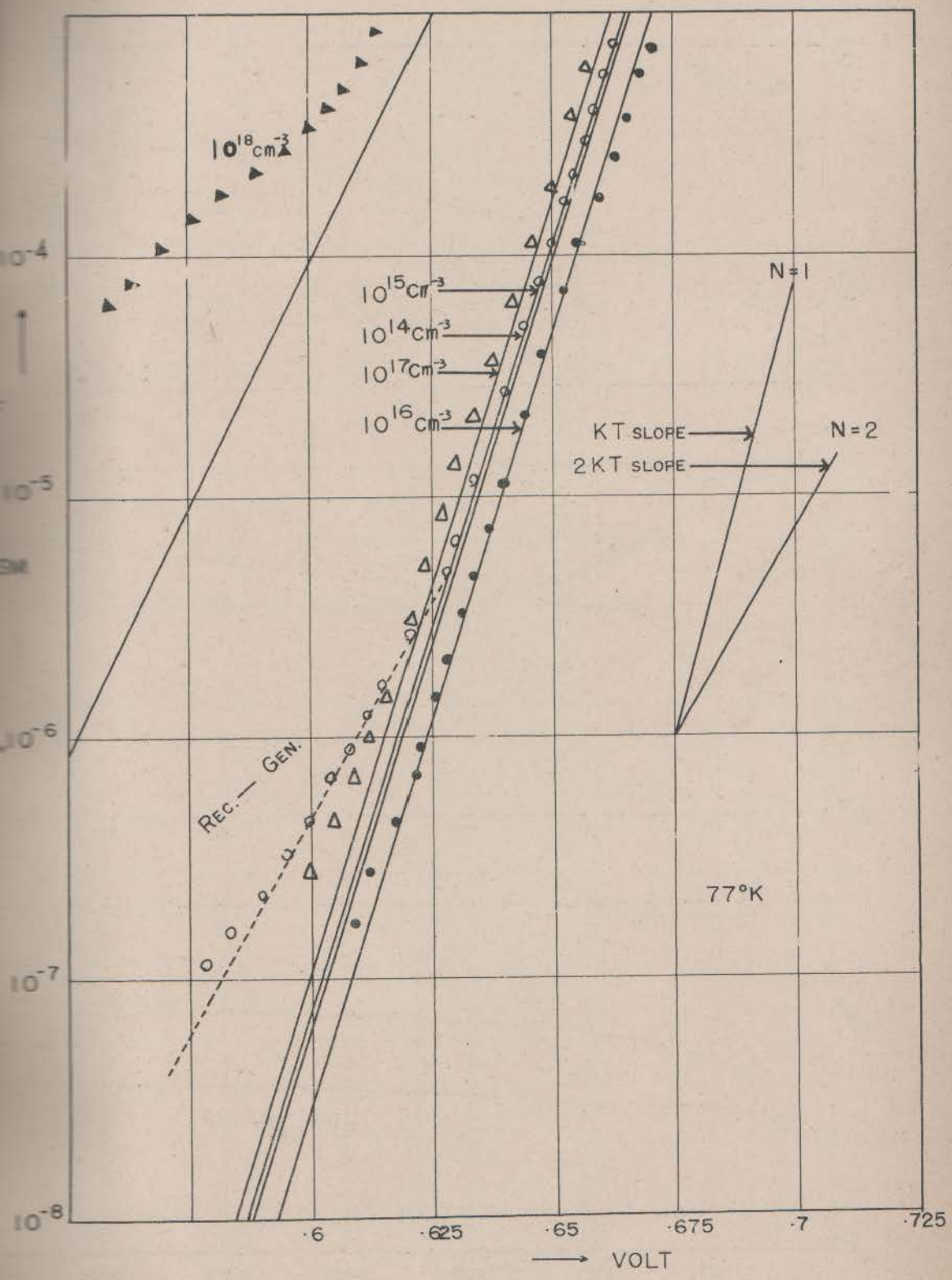


fig. 4. (b) for T = 77°K.

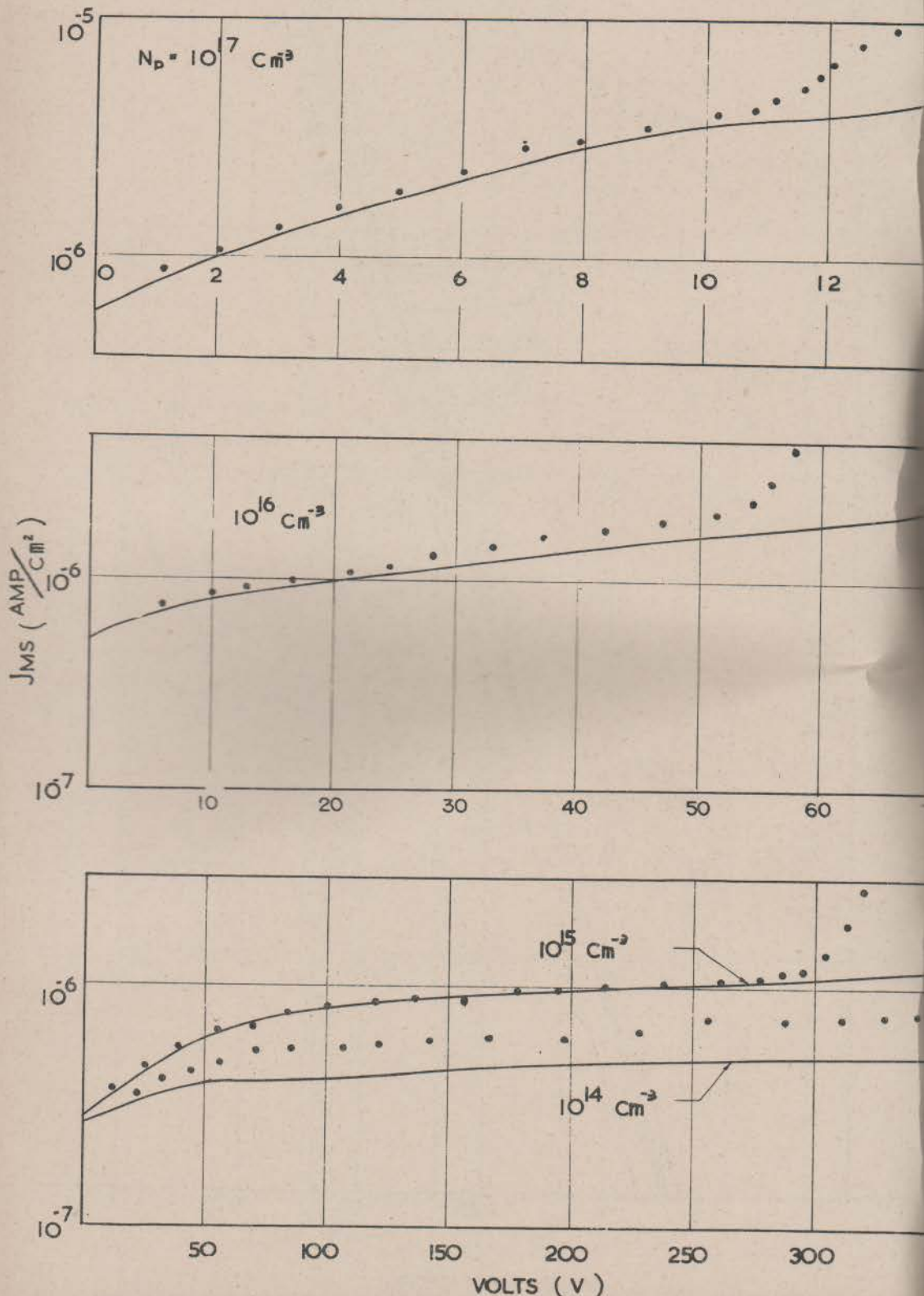


Fig. 5. Theoretical and experimental values of $J_{MS}$ versus reverse bias voltage. Solid lines are the theoretical results while the data points are obtained experimentally.

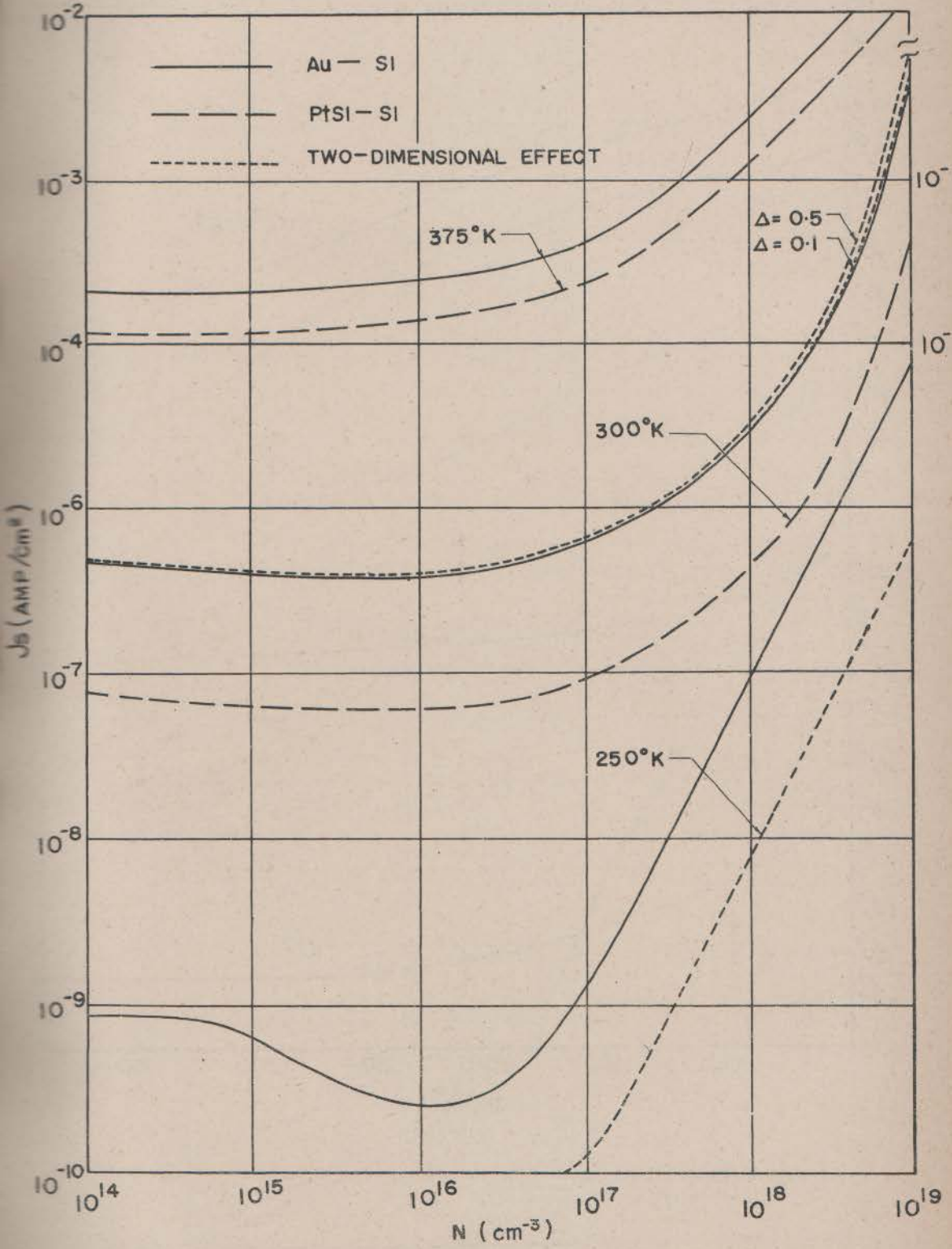


Fig. 6. Saturation current density versus doping with temperature as a parameter. Solid lines are for Au-Si system, dashed lines for PtSi-Si system, and dotted lines are for statistical variation of impurity.

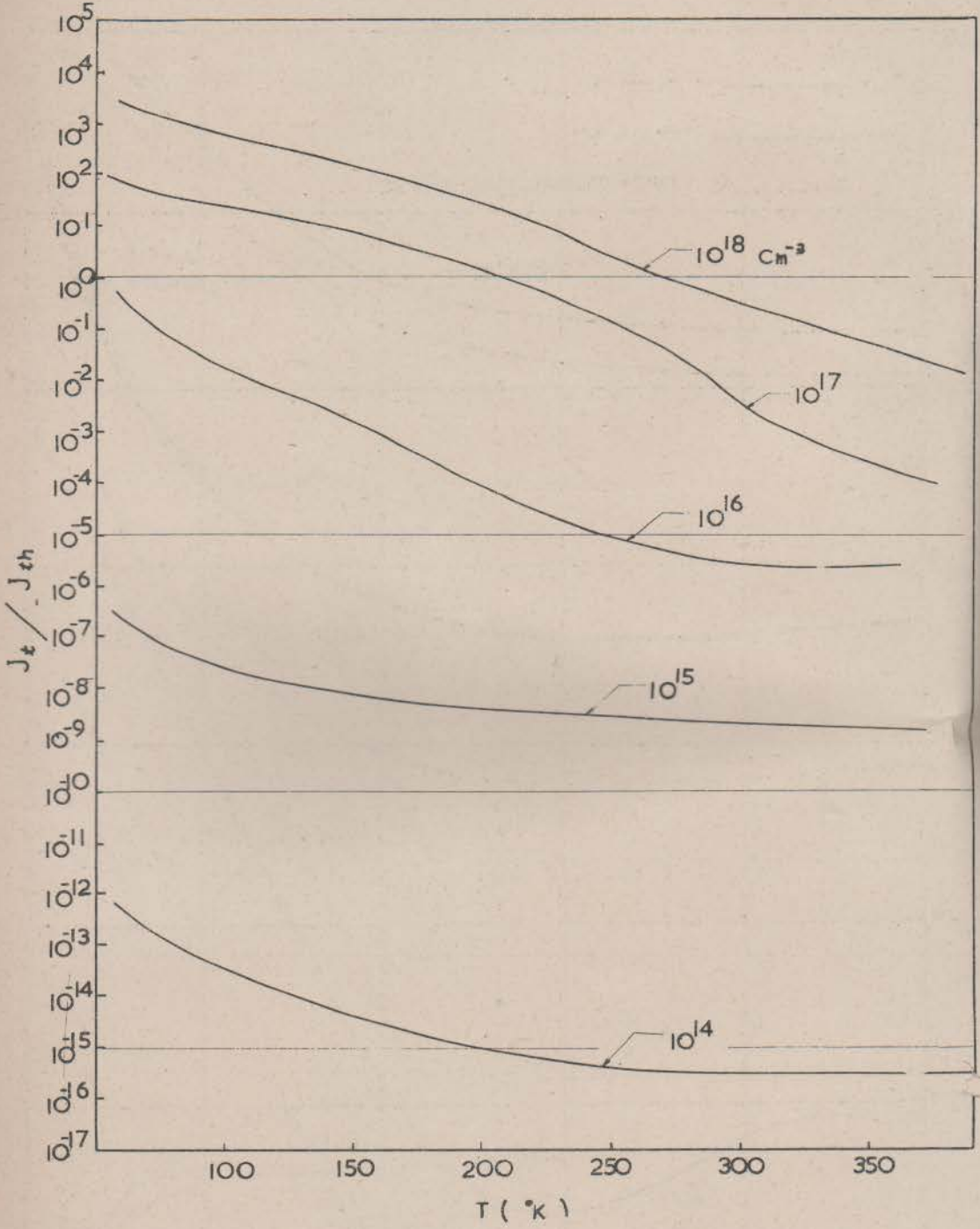


Fig. 7. Theoretical ratio of the tunnel current to thermionic current density.

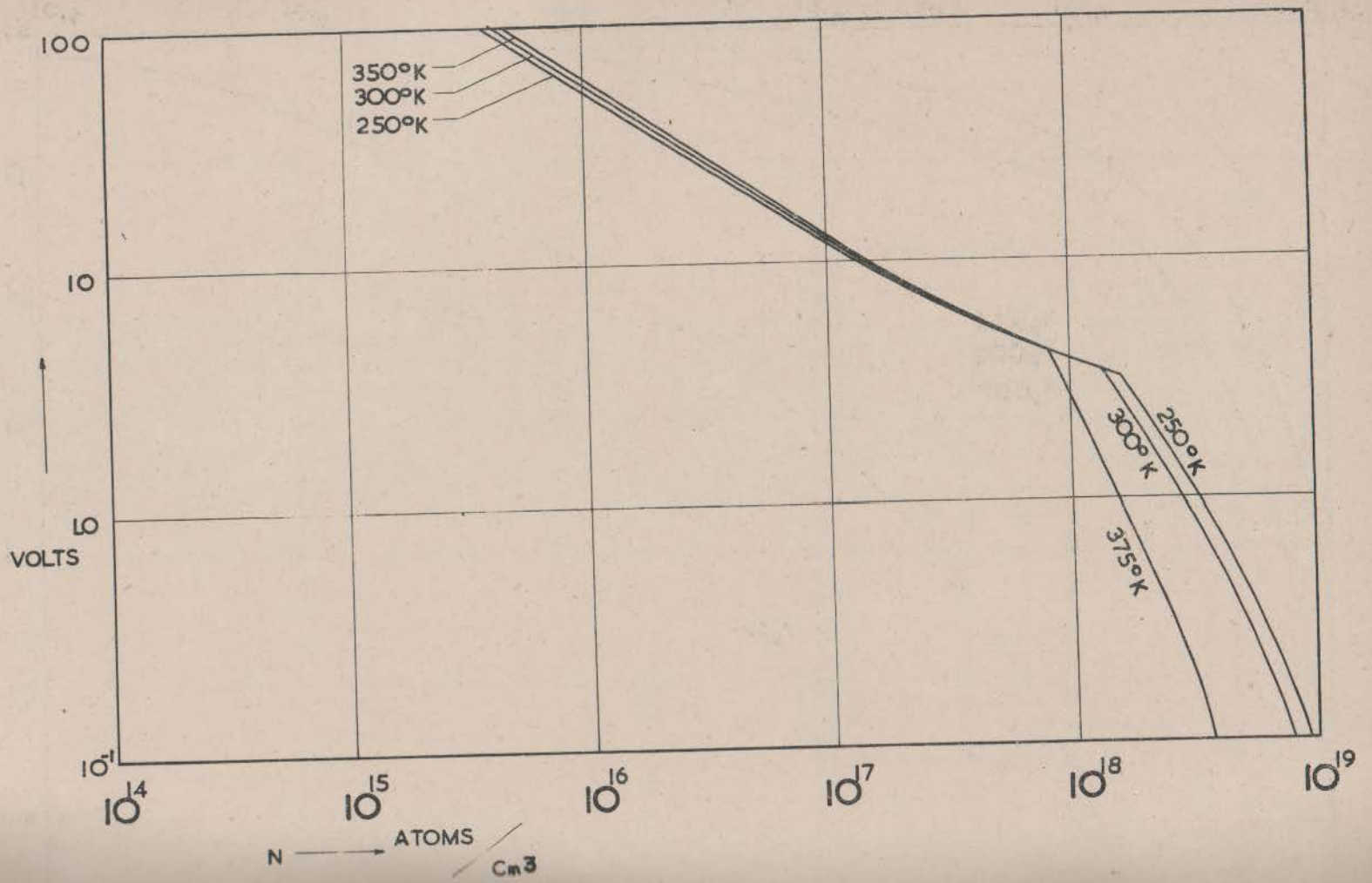


Fig. 8. Breakdown voltage versus doping with temperature as a parameter.

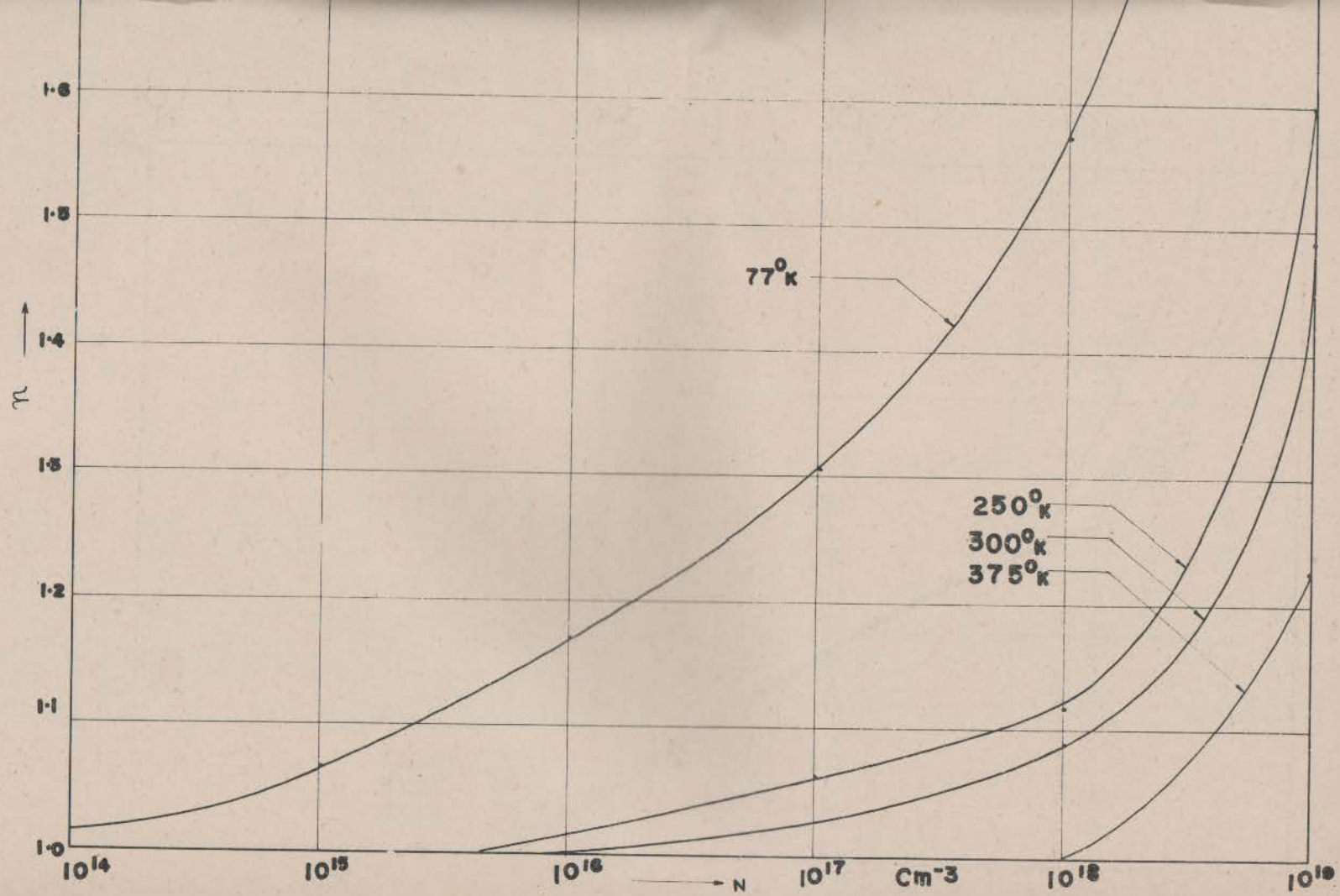


Fig. 9. n versus doping with temperature as a parameter.

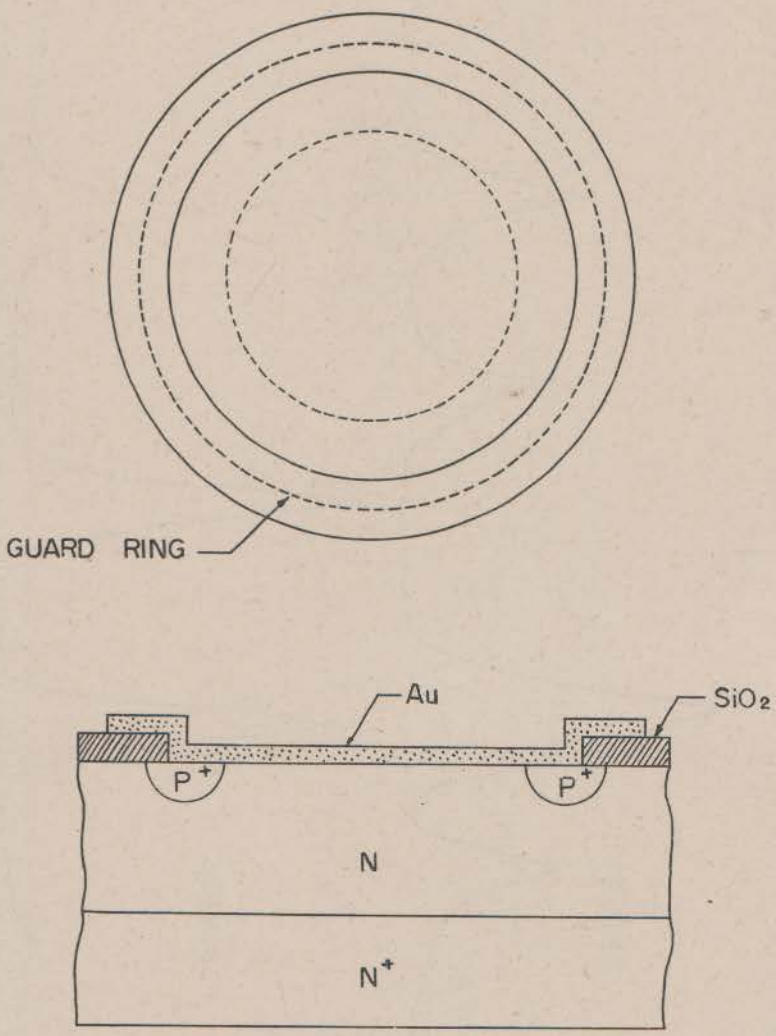


Fig. 10. Device geometry of a Schottky barrier diode.

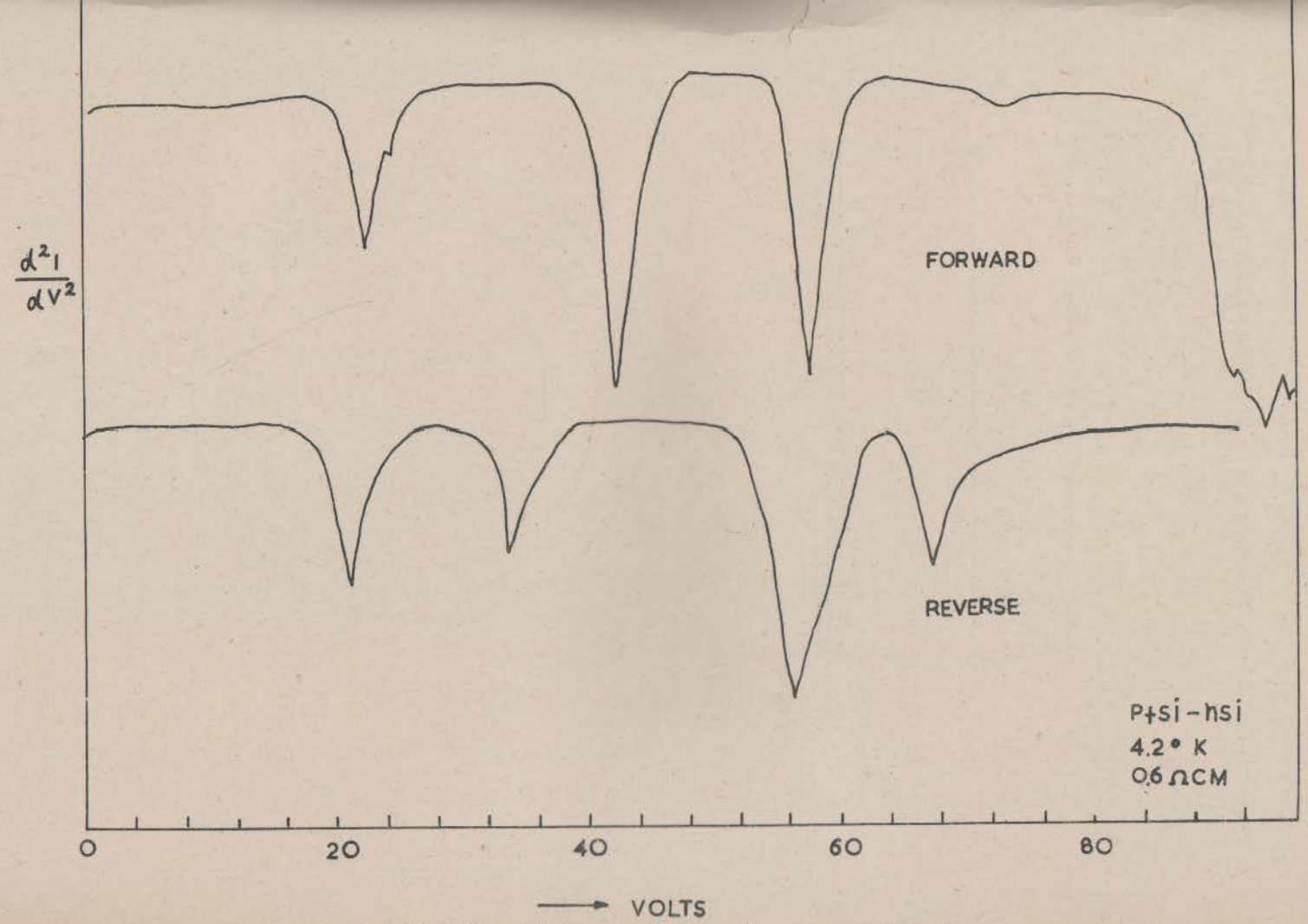


Fig. 11. Differential conductance peaks versus voltage for (a) PtSi-Si diode and

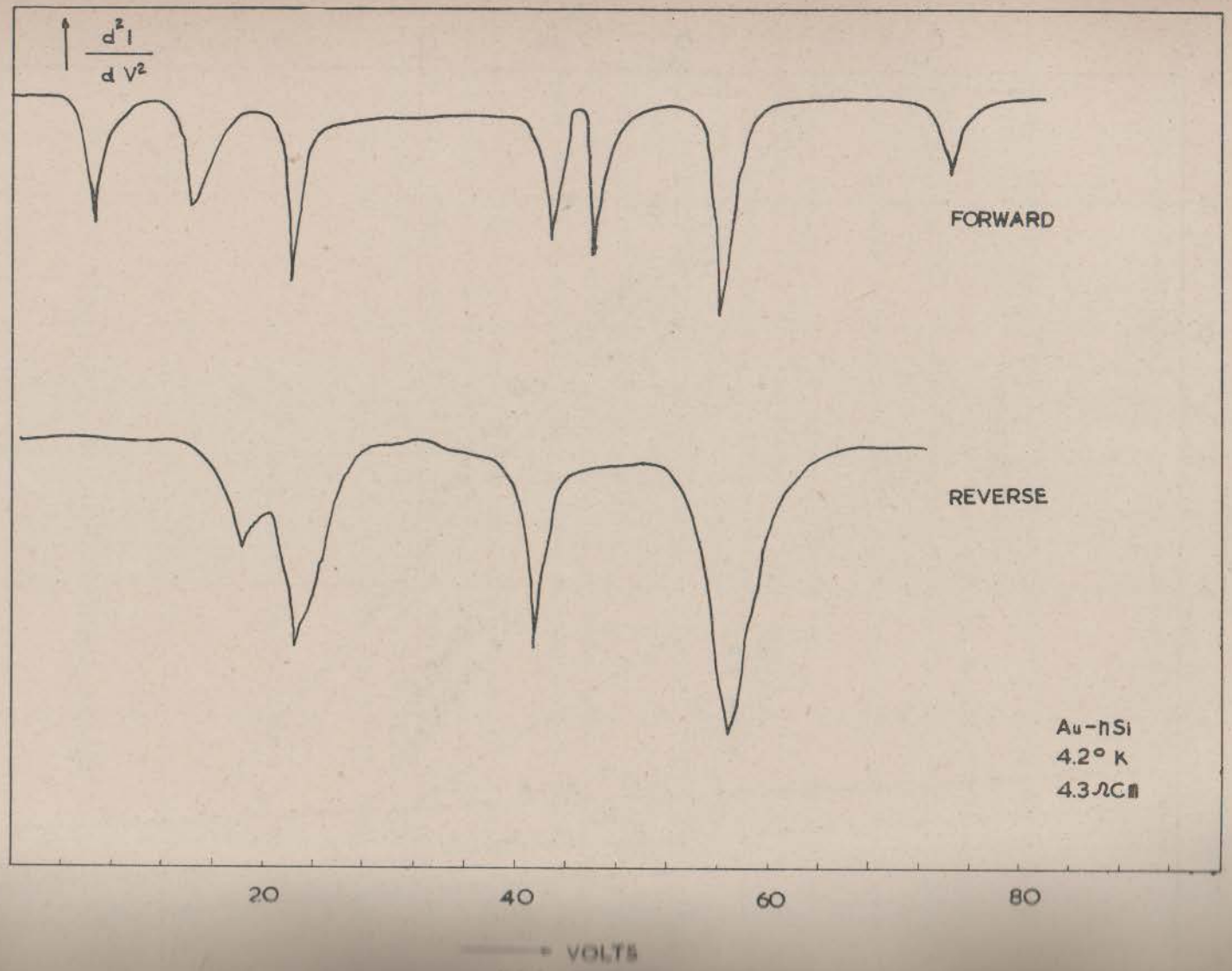
$\frac{d^2I}{dV^2}$
FORWARD
REVERSE
Au-nSi
4.2° K
4.3Ω cm
20
40
60
80
VOLTS

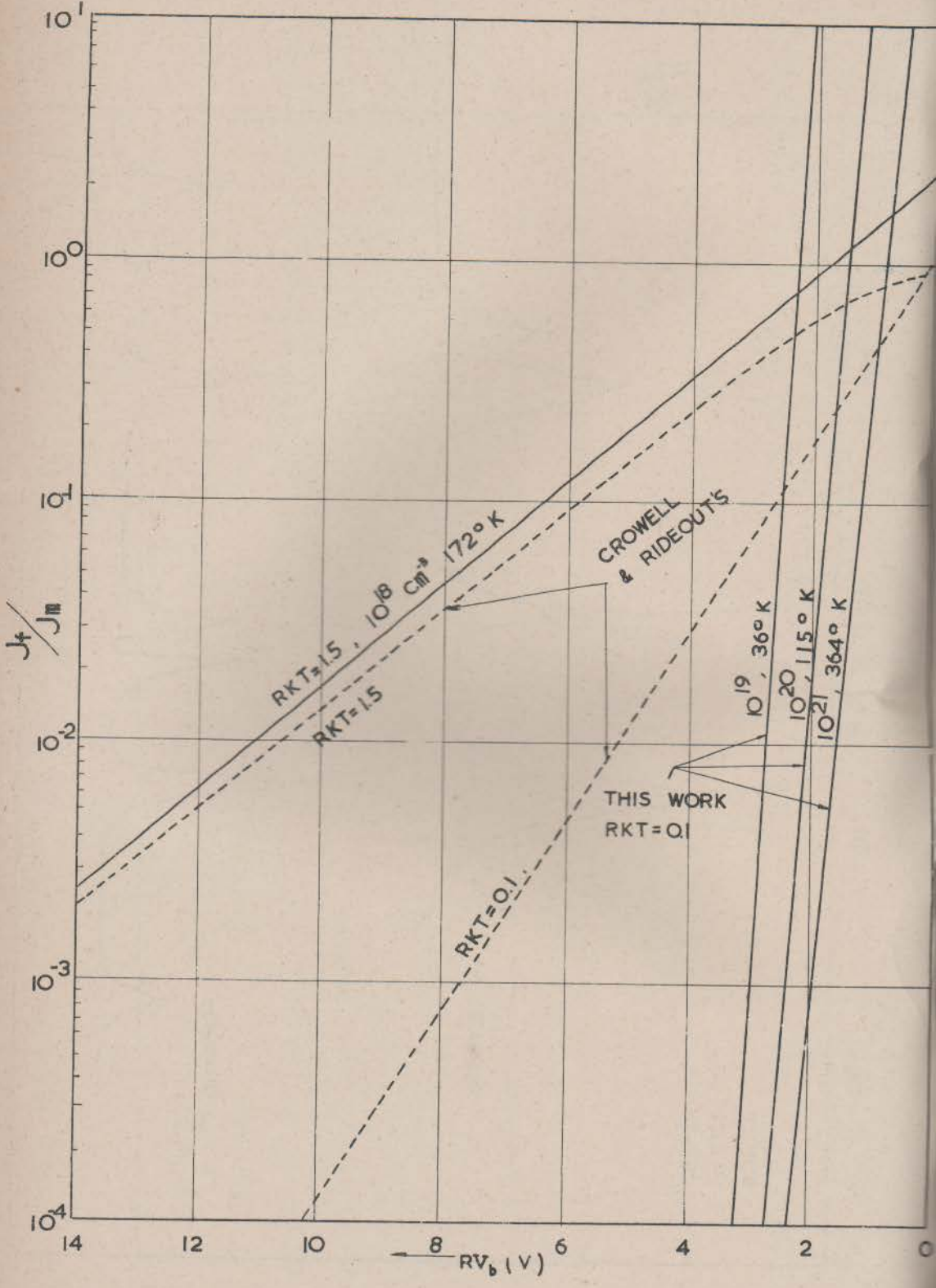


Fig. 12. Comparison of the present theory with that of Crowell and Rideout's